Experimental determination of different saturation functions for simulation of underground geological CO_2 storage

Bettina Jenei[1,], Mohammed Al-Eryani[1], Roman Manasipov[2], and Leonhard Ganzer[1]*

[1]TU Clausthal, Institute of Subsurface Energy Systems, 38678 Clausthal-Zellerfeld, Germany
[2]Datagration Solutions Inc., 2500 Baden, Austria

Abstract. Relative permeability and capillary pressure saturation functions are essential for understanding and characterising multiphase fluid flow through porous media. These saturation functions determine the efficiency of water flooding, and energy and gas storage operations on a microscopic and macroscopic scale. During CO_2 storage, these serve as essential input parameters in numerical reservoir simulation studies to determine storage capacity, caprock integrity and to predict fluid flow movements in the reservoir. There is limited information on the saturation functions for CO_2-brine systems under different reservoir conditions, especially in the context of geological storage of CO_2. Unlike immiscible fluid flow, various displacement fronts can occur during CO_2 storage in the same formation, because the amount of dissolved CO_2 in the aquifer is time and location dependent. Therefore, the reservoir could be divided into flooding zones based on the amount of free and dissolved CO_2. The goal of this paper is to investigate the impact of dissolved CO_2 in the water phase on the saturation functions. These results will then be used in numerical simulation studies to estimate the storage capacity and improve CO_2 plume development. To investigate these phenomena properly, interpretation of experiments is key to de-risk projects. One must remember that these parameters are measured indirectly; therefore, the measurements require meticulous and precise interpretation techniques. Analytical approaches are used and combined with numerical methods utilising $DuMu^X$ and assisted history-matching techniques.

1 Introduction

With the 'Paris Agreement' at the 2015 World Climate Conference, 195 countries committed to curbing climate change and making the global economy more climate-friendly to limit global warming to a maximum of 2 degrees [1]. At European level, the 'European Green Deal' was presented in 2019 with the aim of reducing Europe's net greenhouse gas emissions to zero by 2050. The effects of these political decisions present the energy sector with challenges that require an extraordinary degree of flexibility. To mitigate the fluctuation of sustainable energy sources, the geological subsurface has an important role to play: the storage of hydrogen or gas mixtures in porous media, the capture and underground storage of carbon dioxide (Carbon Capture and Storage, CCS), the capture, use and storage of carbon dioxide-containing industrial products (Carbon Capture Utilization and Storage, CCUS) are applications based on the technical understanding of multiphase flow of gases and liquids in porous media. This paper presents the development of an experimental setup which is an optimization of core flooding technology. After the experiments are completed, the investigation of the saturation functions of multiphase fluid flows will continue. There is a need for investigation of a range of undersaturated conditions when injecting supercritical CO_2, due to the lack of information in literature on the saturation functions in supercritical-liquid systems, especially for CO_2 storage. Unlike immiscible liquid flow, numerous displacement fronts can occur in underground geological CO_2 storage [2]. For example, the reservoir could be divided into different flooding zones and categorised based on the amount of free and dissolved CO_2 [3]. Therefore, an optimized core flooding apparatus is designed. By using a carbonated-water core-flooding experimental setup, the effect of the amount of dissolved CO_2 in the water phase on the saturation functions can be investigated. If there is a significant relationship, a function can be derived that can be used in numerical simulation studies to correctly interpret the storage capacity and plume motion.

Since not only the fluid distribution but also the sealing efficiency of the caprock is a decisive parameter, additional applications should focus on other critical parameters such as the capillary pressure [3]. To complement the analysis, experimental determination of relative permeability along with the additional multi-scale data acquisition and the application of microfluidic technology and image analysis are planned. The

* Corresponding author: bettina.jenei@tu-clausthal.de

resolution and the uncertainty of the measurement data limit the analysis process, since the measured values are further used in the analytical or numerical formula. Consequently, in addition to the experimental setup, the applied interpretation technique plays an important role in understanding the multiphase fluid flow in CO_2 sequestration. The strategy, the theory and the mathematical background behind the relative permeability matching in a core model is similar to conventional history matching. The model uses observed and control data, like in a field model, but with fewer parameters and faster computation. The number of parameters is smaller than in field simulation, therefore, the relative permeability can be matched accurately. The simultaneous matching technique improves interpretation of SCAL data by imposing greater control and constraints on model parameters through combining multiple experiment types, thereby narrowing the range of acceptable solution [4]. Combining steady-state and centrifuge experiments is suggested for an adequate interpretation based on simulated results.

2 Objectives and literature review

The relative permeability and the capillary pressure curves are describing the behaviour of the multiphase flow in the reservoir. Displacement and sweep efficiency are determined by these functions. Key characteristics of relative permeability curves are irreducible saturations, end points and curvature. They describe multiphase flow behaviour within specific saturation ranges in the reservoir. For this reason, they serve as an input for reservoir simulations of CO_2 storage. Dynamic reservoir behaviour of CO_2 storage will be governed by absolute and relative permeabilities. These permeabilities, along with Darcy velocity, control the flow path and speed (advective part of the flow). The absolute and relative permeability appear in Darcy velocity together as a product, which is called effective permeability $k_{eff} = k \cdot k_r$. Changes in absolute permeability affects all phases, while changes in relative permeability affect only the selected phase. Effective permeability can mimic diverse reservoir fluid flow behaviour but have risks of violating the assumptions and introducing inconsistencies, potentially creating unfeasible predictive scenarios.

Capillary pressure has a significant effect on the saturation distribution (local fluid volumes) after the CO_2 injection phase, and as a part of Darcy velocity, affects the flow path (the diffusive part of the flow). Therefore, it can also mimic a wide variety of flow patterns. In addition, in the case of using unrealistic saturation functions, the volumetric part of the cell can be compensated by unfeasible values, which influences the outcome of the prediction (primarily for pressure). It introduces the wrong model with incorrect fluid volumes spatially, which leads to unrealistic prediction scenarios on the movement of CO_2 plume.

Modelling CO_2 storage consist of two phases, operation and post-closure phase. Subsequently, the influence of capillary and gravity forces is not fully present. Moreover, when injection phase stops, capillary pressure significantly impacts simulation results. However, if the prediction phase is dominated by injection, viscous forces prevail, and capillary pressure plays a minor role. Therefore, in the viscous dominated regime, the fluxes are proportional to a pressure gradient (pressure difference) between reservoir and injection wells, and the flow direction is initiated from injection well towards the reservoir. In 2015, the global CCS institute published a compilation of all reported drainage CO_2-brine relative permeability measurements, where many experiments were performed at repeat conditions, with different rock samples [5]. All of the relative permeability curves superimposed onto one plot, are shown in Fig.1., where the measurements are done with brine without dissolved CO_2.

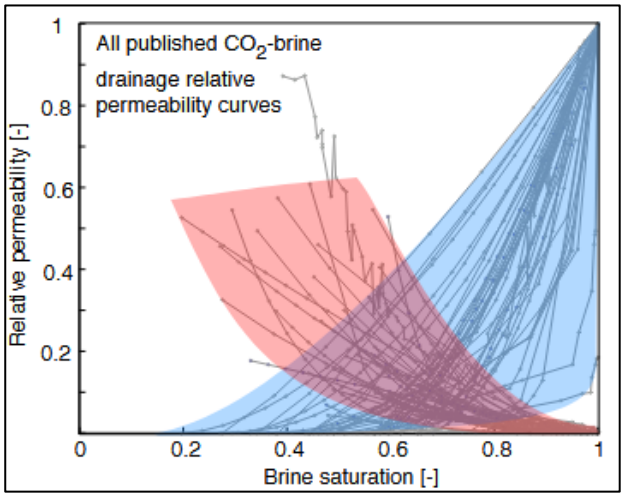

Fig. 1. All published CO_2-brine drainage relative permeability curves [5]

As a result, to tackle the lack of information on relative permeability between CO_2 saturated brine and CO_2, additional experiments must be carried out [2]. The main objective of this paper is to design and test a measurement to identify and characterise different saturation regions by representative relative permeability functions, focusing on the impact of different amount of dissolved CO_2 (under the same pressure and temperature conditions) on the saturation function, namely relative permeability [6].

Understanding the relative permeability of CO_2-brine systems is essential not only for optimizing carbon capture and storage (CCS), but also to optimise enhanced oil recovery (EOR) processes [3]. Several key studies have focused on measuring relative permeability using brine saturated (pre-equilibrated) with CO_2, reflecting the in-situ conditions post-CO_2 injection.

Müller (2010) described the measurement of relative permeability in the laboratory, typically using either steady-state or unsteady-state methods. It was noted that

these setups typically do not use brine pre-saturated with CO_2 (referred to as "live brine"), even when investigating supercritical conditions [7]. Krevor et al. (2012) conducted an experimental investigation into the multiphase flow properties of CO_2 and water in four distinct sandstone rocks, including Berea sandstone and three reservoir rocks. Measurements in the Berea sample aligned with past studies using both CO_2/brine and oil/water systems. These measurements were conducted above the critical point for CO_2 but did not mimic and cover undersaturated conditions [8]. Chen et al. (2014) investigated CO_2-brine relative permeability in a Berea sandstone core at conditions where CO_2 exists in a liquid phase. The brine and CO_2 were saturated with each other to prevent mass transfer during the experiments. The measured conditions (below the critical point of CO_2) do not mimic the real injection conditions, where the CO_2 is in supercritical state [9]. Jeong et al. (2021) examined the impact of flow rate on the relative permeability curves in CO_2-brine systems, focusing on Berea sandstone, in geological storage of CO_2. The study highlights the importance of understanding the relative permeability for optimizing CO_2 storage in geological formations, which is critical for carbon capture and storage (CCS) applications. The findings suggest that optimizing flow rates is crucial for enhancing CO_2 storage capacity and injectivity [10]. Moore et al. (2021) investigated the relative permeability of supercritical CO_2 ($scCO_2$) and brine using an unsteady-state flow method combined with computed tomography (CT). The study aims to provide a rapid and efficient method for determining relative permeability for CO_2 storage in geological formations [2]. Ge et al. (2022) investigated the influence of capillary pressure boundary conditions and hysteresis on CO_2-water relative permeability using unsteady-state experiments and numerical simulation. The study aims to provide more accurate estimates of relative permeability, which is crucial for CO_2 injection processes in enhanced oil recovery and carbon sequestration. The study concludes that incorporating capillary pressure boundary conditions into the JBN method enhances the accuracy of relative permeability estimates, thereby improving the reliability of CO_2 storage capacity and injectivity predictions [11].

The current research aims to fill the gap left by previous studies, with utilising their findings and recommendations. Measurements are conducted with saturated and initially undersaturated distilled water and brine samples and at supercritical conditions. The goal is to determine CO_2 saturation functions in the different regions to eventually predict the CO_2 plume behaviour along with the CO_2 storage capacity using improved interpretation methods mentioned in this paper. By addressing both saturated and undersaturated conditions, this study highlights the need for a more comprehensive understanding of CO_2-brine interactions. Moreover, to tackle their effect on multiphase fluid flow characteristics and to enhance the accuracy of CO_2 storage predictions. The developed setup enables core initialisation under various saturation conditions by incorporating a saturation unit. This unit saturates water samples with CO_2 at different pressures and temperatures, mimicking the CO_2 solubility at reservoir conditions. The pressure and temperature of the entire setup are matched to the saturation conditions to maintain CO_2 in solution during the core flooding.

3 Materials and Methods

3.1 Materials

The rock sample used in the conducted measurements were Bentheimer sandstone with measured porosity of 25% and approximately 2000mD absolute permeability. The utilised fluids are supercritical CO_2 with 99.9% purity and distilled water. The salinity is influencing the amount of dissolved CO_2 in the water. Therefore, as a starting point distilled water was used for the core floods, but both distilled and saline water for the viscosity measurements.

For the viscosity measurements, water samples can be prepared to match the expected aquifer salinity. Specifically, for the viscosity measurements water samples were prepared with a salinity of 20% (20 wt% NaCl) to represent aquifers in the North German Basin. Each sample was stirred for 20 minutes to ensure consistent salt dissolution conditions. The properties of carbonated water are crucial as accurate interpretation of saturation functions (relative permeability and capillary pressure) depends on the fluid properties like density and viscosity. Fig.2 shows the conditions at which relative permeability experiments between brine and CO_2 are conducted and reported in literature.

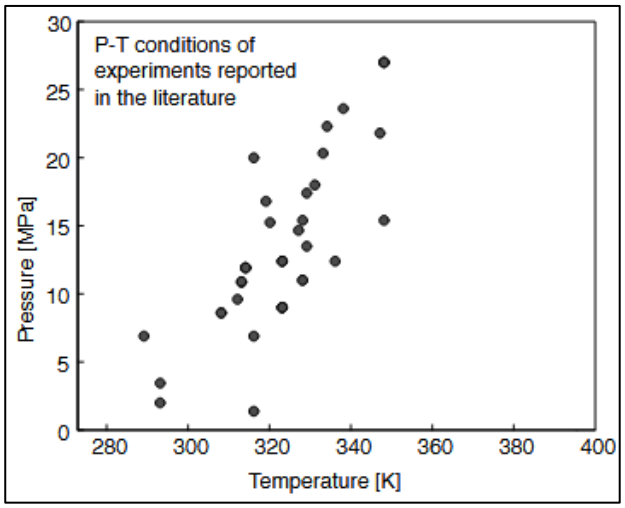

Fig. 2. P-T conditions of relative permeability experiments between brine and CO_2 reported in the literature [5]

Nonetheless, as mentioned previously, the measurements found in literature are not investigating different range of CO_2 saturated brines at the same pressure and temperature conditions.

3.2 Methods

3.2.1 Viscosity measurement of carbonated water/brine

The dynamic viscosity was experimentally determined by measuring the pressure drop across a coiled capillary tube, using a differential pressure sensor to record this change, shown in Fig. 3. The experiment started by filling the piston accumulator with the brine sample. The system's temperature was then adjusted to the required level and was allowed to stabilize. After this, CO_2 was injected into the system using a syringe pump (ISCO). This method helped determine the pressure loss through coiled capillary at the desired absolute pressure. Once the system reached the desired temperature, the brine was pushed through the setup, including the capillary tube which has specific dimensions. As the brine flowed through this tube, it led to a drop in pressure, which was recorded by a differential pressure sensor connected at the inlet and outlet of the tube. Once the pressure difference stabilized, the value is used to determine the dynamic viscosity from the Hagen Poiseuille equation [12].

$$\Delta p = \frac{8\mu LQ}{\pi R^4} \quad (1)$$

Where Δp is the pressure difference between the inlet and outlet of the coiled capillary, μ is the dynamic viscosity, L is the length of the capillary, Q is the flow rate and R is the radius of the capillary.

The main difference between measurements of brine with CO_2 and without is in the preparation. The CO_2-saturated brine samples were left overnight to ensure they were fully saturated. For brine samples without CO_2, the measurement was run right after the brine samples reached the desired temperature, which usually took two to three hours after filling the piston accumulator, the process of injecting the sample began by turning a three-way valve that connected the piston accumulator to the rest of the system.

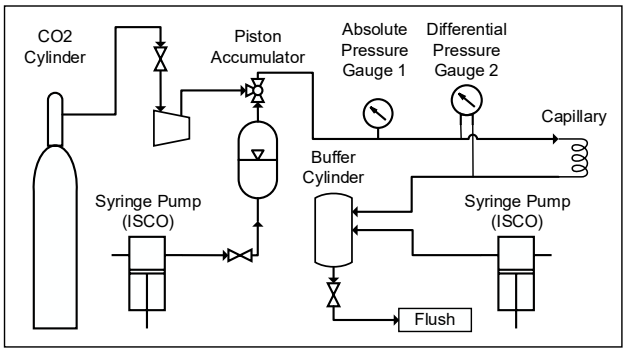

Fig. 3. CO_2 Experimental setup for dynamic viscosity of CO_2 saturated liquid sample (carbonated water)

3.2.2 Unsteady-state measurement method and analytical interpretation of relative permeability

The relative permeability of rock for each fluid phase can be measured in core samples by either steady-state (SS) or unsteady-state (USS) techniques or centrifuge. Since the measurements conducted were USS, it is briefly explained. The most accurate method to measure the relative permeability is the Steady-State (SS) method, but it is time consuming and requires costly resources. Another method that is frequently used to investigate the relative permeability is under unsteady state conditions (transient), which means that the measured variables are time-dependent. USS relative permeability can be experimentally determined under ambient (slightly elevated pressure and temperature conditions) or under reservoir conditions (more rarely). As an advantage, USS measurements are typically much faster to perform than SS. Furthermore, the injection rate and the fluid properties must remain constant. In addition, the pressure gradient must be large enough to neglect capillary pressure effects. Considering fluid compressibility is important when interpreting results, as relative permeability is an indirect measurement heavily influenced by data analysis [13]. When CO_2 is supercritical, compressibility is insignificant at the operating pressure, unlike when CO_2 is gaseous. These assumptions are crucial for reliable experimental design and result interpretation. Several analysis techniques have been proposed to derive the relative permeability from unsteady-state core floods. As previously mentioned, the unsteady state experiment has a main advantage, which is that the measurement procedure is faster and less complex than the SS relative permeability technique. The main disadvantage arises from the analytical model, which implies some complexity in combination with crude assumptions, namely incompressible, immiscible multiphase fluid flow and neglected capillary pressure between the wetting and non-wetting phase, with the assumption of constant injection rate. The mathematical approach which is used for interpretation of the unsteady-state experimental results is the Buckley–Leverett theory extended by Welge [14]. Moreover, Johnson-Bossler-Naumann (JBN) method is summarised in the following [15].

The phase velocities $u_w(L,t)$ and $u_{nw}(L,t)$ at the outlet at time t (production rates):

$$u_w(L,t) = \frac{1}{A}\frac{dQ_w}{dt} \quad (2)$$

$$u_{nw}(L,t) = \frac{1}{A}\frac{dQ_{nw}}{dt} \quad (3)$$

Saturation $S_w(L,t)$ at the outlet at time t :

$$S_w(L,t) = S_{wc} + \frac{1}{AL\phi}\left(t\ \frac{dQ_w(t)}{dt} - Q_w(t)\right) \quad (4)$$

Relative permeability ratio:

$$\frac{k_{rw}(S_w(L,t))}{k_{rnw}(S_w(L,t))} = \frac{\mu_w}{\mu_{nw}} \frac{u_w(L,t)}{u_{nw}(L,t)} \quad (5)$$

Relative permeabilities:

$$k_{rw} = \frac{\mu_w L u_w(L,t)}{K} \left(\Delta P(t) - t \frac{d(\Delta P(t))}{dt} \right)^{-1} \quad (6)$$

$$k_{rnw} = \frac{\mu_{nw} L u_{nw}(L,t)}{K} \left(\Delta P(t) - t \frac{d(\Delta P(t))}{dt} \right)^{-1} \quad (7)$$

Buckley-Leverett equation:

$$-\frac{df_w}{dS_w}\frac{\partial S_w}{\partial x} = \frac{A\phi}{q}\frac{\partial S_w}{\partial t} \quad (8)$$

To solve this equation, the method of characteristics is applied. Each characteristic line represents a path of constant saturation $S_w(x,t)$. The full differential of saturation can be written as:

$$dS_w = \frac{\partial S_w}{\partial x} dx + \frac{\partial S_w}{\partial t} dt \quad (9)$$

Since the velocities of constant saturations are of interest, the full differential becomes zero:

$$0 = \frac{\partial S_w}{\partial x} dx + \frac{\partial S_w}{\partial t} dt \quad (10)$$

Substituting it to Buckley-Leverett equation, gives us velocities of saturations, including the one at the front:

$$\frac{dx}{dt} = \frac{q}{A\phi}\frac{df_w}{dS_w} \quad (11)$$

Integrating both sides over time from $t = 0$ to $t = t$:

$$\int_{t=0}^{t=t} \frac{dx}{dt} dt = \int_{t=0}^{t=t} \frac{q}{A\phi}\frac{df_w}{dS_w} dt \quad (12)$$

From which results, one gets the position of each saturation at time t, including the one at the front:

$$x_f = \frac{qt}{A\phi}\left(\frac{df_w}{dS_w}\right) \quad (13)$$

where fractional flow function can be calculated as:

$$f_w = \frac{1}{1+\frac{k_{ro}}{k_{rw}}\frac{\mu_w}{\mu_0}} \quad (14)$$

The implementation of the described calculation sequence can be accessed through online repository on github page [16]. In case of the CO_2 injected as a gas phase during the experiments, it can also be interpreted with the analytical JBN method described above. The JBN formulation then needs to consider the compressibility of the injected displacing phase. In addition, the miscibility and the capillary pressure [11] between the displaced and displacing phase should be considered. The extension of the analytical approach beyond the Buckley Leverett assumptions is challenging and would work under other set of assumptions. Therefore, the use of numerical solution is preferred. Since, it is reduced to a one-dimensional problem, it is fast, accurate and therefore efficient. It also can be further generalised to be applicable for more complex fluid flow, including incompressible and multi-phase multi-component. Therefore, it can be used for the interpretation of relative permeability functions of other fluid systems such as in hydrogen storage applications.

3.2.2 Mathematical model of unsteady state experiment

An unsteady state core-flooding experiments conventionally for an oil-water system can be modelled under the assumption of an incompressible immiscible flow. These assumptions are also applied in this study. The following system of equations describes it:

$$\phi \frac{\partial \rho_\alpha S_\alpha}{\partial t} - \nabla \cdot \left(\rho_\alpha \frac{k_{r\alpha}(S_\alpha)}{\mu_\alpha} \boldsymbol{K} \cdot (\nabla p_\alpha - \rho_\alpha \boldsymbol{g}) \right) - \rho_\alpha q_\alpha = 0 \quad (15)$$

$$p_c(S_w) = p_w - p_n \quad (16)$$

$$\mathbf{v}_\alpha = -\frac{k_{r\alpha}(S_\alpha)}{\mu_\alpha} \boldsymbol{K} \cdot (\nabla p_\alpha - \rho_\alpha g) \quad (17)$$

$$\mathbf{v}_\alpha A \cdot \boldsymbol{n} = q_\alpha^{inlet} \quad (18)$$

$$p_\alpha = p_D^{outlet} \quad (19)$$

Where ϕ, k are the porosity and absolute permeability of the core sample; $\alpha = \{w, n\}$ is wetting and non-wetting phase respectively; ρ_α, μ_α, S_α, p_α are the phase density, dynamic viscosity, saturation and pressure; q_α are the source/sink terms; kr_α is the relative permeability of associated phases; v_α Darcy's velocity of individual phases. The boundary conditions for the unsteady-state experiment can be set using the Neumann condition or source term on the inlet by specifying the injection rate of the displacing phase, and by setting the Dirichlet boundary condition on the outlet by specifying the backend pressure. It is common for modelling the core-flooding experiments to define an inlet and outlet blocks [17] with zero capillary pressure and linear relative permeabilities, which in actual experiment represent mixing sections typically with 'spyder web' groove pattern to promote flow mixing and reduce capillary end effect [18]. For the numerical interpretation the DuMu^X simulator [19,20] was selected, which is well suited for the modelling of multiphase multicomponent flow in porous media, capable of modelling pore network flow and solving Navier-Stokes equations using a phase field approach for capturing the interfaces of several phases. This opens up great opportunities to adapt interpretation routines to various fluid systems and experimental setups. In addition, DuMu^X has already been used to develop the SCORES simulator [18], which is freely available for performing simulation runs, but it is not provided with the corresponding source code. As a result, the DuMu^X open source code for core-flooding used in this work will be released to fill this gap. Additionally, the corresponding open-source Python package [21] will include the interpretation methods presented in this paper. Additionally, there are other efficient open-source tools available for interpreting of SCAL experiments [22].

3.2.3 DuMu^X vs. SCORES Benchmark

Based on a thorough and extensive benchmark study of four simulators, SCORES, SENDRA, PORLAB, and CYDAREX [23,24], an unsteady state experiment (Case-3) was chosen to validate the simulation model.

The injection schedule setup is defined in Table 1 and the core sample and fluid properties are listed in Table 2. The relative permeabilities have endpoints $kr_w^{max} = 0.5$ and $kr_n^{max} = 0.5$, and Corey exponents $c_w = 3$ and $c_n = 3$ corresponsingly.

Table 1. Injection schedule.

Time (hour)	Q water (cm3/hour)
10	1
13	10
16	70
21	200
26	300

Table 2. Core sample and fluid properties.

Property	Value
core length [cm]	8
core diameter [cm]	4
core permeability [mD]	100
water viscosity [cP]	1
water density [g/cm^3]	1
oil viscosity [cP]	5
oil density [g/cm^3]	0.8
initial water saturation	0.2
final water saturation	0.8

As shown in Fig. 4. and 5, the results for the differential pressure and average saturation in the core are practically identical. The following benchmark results are expected because both results are based on the DuMu^X simulator; however, the results from SCORES were published based on at least an eight years older version of DuMu^X code.

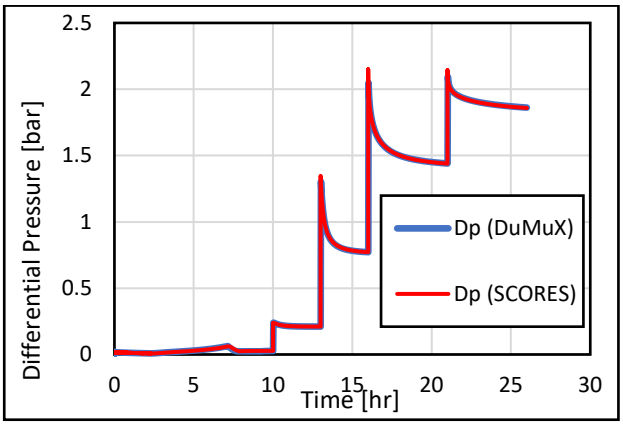

Fig. 4. Differential pressure. Unsteady state simulation benchmark DuMu^X vs. SCORES (DuMu^X) (Case-3)

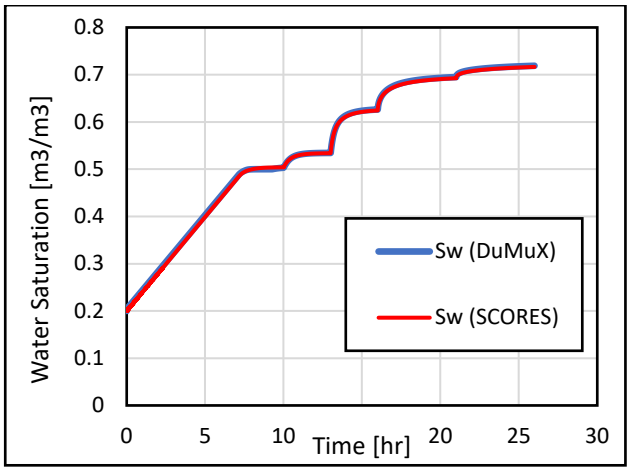

Fig. 5. Average water saturation along the core. Unsteady state simulation benchmark DuMu^X vs. SCORES (DuMu^X) (Case-3).

3.3 Core-flooding experimental apparatus including liquid saturation unit

As mentioned previously, a saturation unit was incorporated to the traditional un-steady state experiment to prepare samples at saturation conditions expected in aquifers. It is possible to adapt the experimental setup of traditional core flooding facility with a separator and piston accumulator for conducting and interpreting SCAL measurements with carbonated water as the displaced fluid. Fig. 6 shows the design of the experimental setup. Experiments based on USS method are frequently used to investigate relative permeability in this work. In this case, it means that the measured variables (differential pressure and cumulative production) during the experiments are time dependent. As it is mentioned previously, the USS measurements are typically much faster to perform, but have couple of constraints in comparison to the steady state method.

Bentheimer sandstone sample is used in the experiments as a rock core. The injection rate and fluid properties remained constant. The mass-transfer between the water and CO_2 phase were neglected in this work. An additional goal of this work is to investigate different saturation regions in the reservoir, where keeping the fluid properties constant is challenging and essential. As a result, different samples with different amounts of dissolved CO_2 should be prepared by varying saturation pressure and temperature of the samples and conducting the measurements at these pressures and temperatures. The fluid properties of the prepared sample (carbonated water) such as density and viscosity could only be maintained through the integration of the fluid saturation unit into the core-flooding apparatus. The closed system is designed to prevent condition changes and therefore avoid CO_2 liberation from solution and from disturbance to the equilibrium thereby keeping the carbonated water's properties constant.

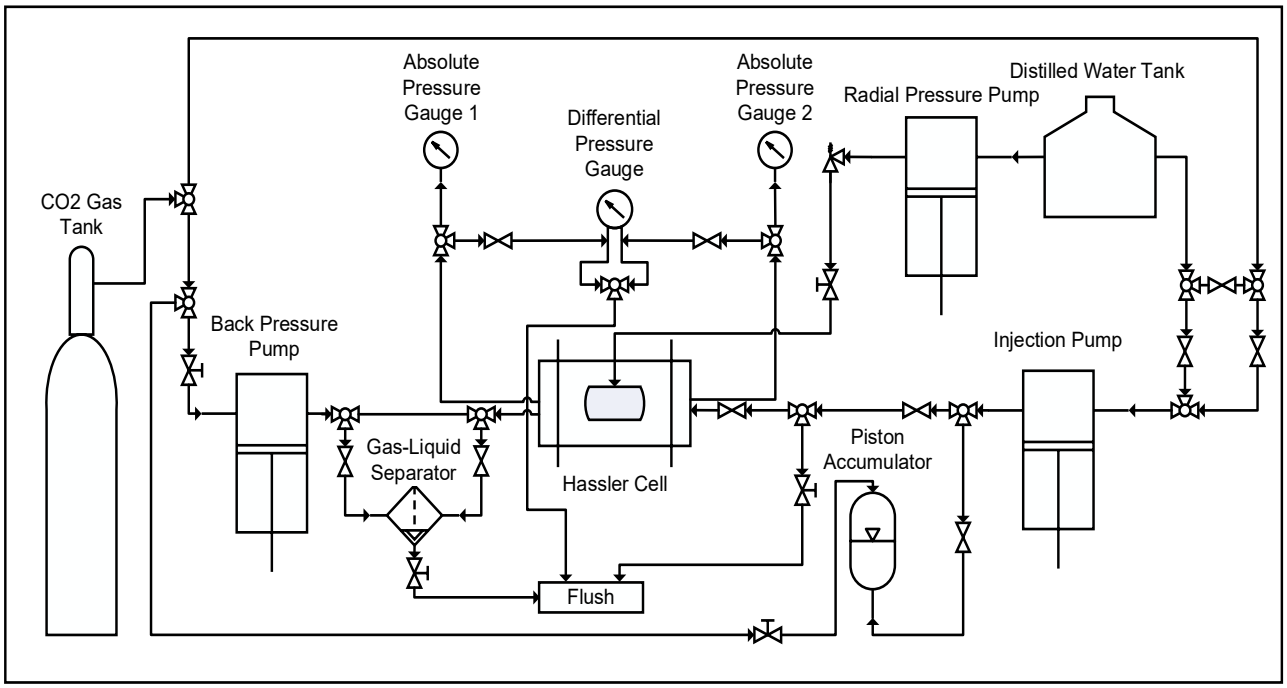

Fig. 6. Design of the Core-flooding experimental apparatus including liquid saturation unit

3.3.1 Design of integrated fluid saturation unit

The integration of the liquid saturation unit into the core-flooding apparatus as a closed system is vital to conduct multiphase flooding experiments for the planned purpose in order to have the aqueous phase saturated and initially undersaturated with the CO_2. The main objective is to maintain a desired amount of CO_2 being dissolved inside the aqueous phase while initialising and conducting the experiments. Prior to the initialisation (saturating it with 100% carbonated water) and the experimental phase an additional phase called liquid saturation phase needs to be carried out. The liquid saturation process is taking place in a piston accumulator which is first filled with the desired water (distilled/brine) and sealed. A syringe pump was then used to inject CO_2 into the piston accumulator containing the water. Subsequently, the saturation valve is opened to introduce the CO_2 to the sample vessel, utilising the CO_2 being pumped by the syringe pump. The cell is then pressurised to the predetermined pressures and brought to the desired temperatures. As CO_2 dissolves in the water sample, the pressure within the vessel decreases. In order to counteract this, the syringe pump, set to "constant pressure mode", compensating for the dissolved CO_2 by pumping additional CO_2. This process continues until the fluid sample reaches equilibrium, fully saturated at the specified pressure and temperature. The illustration of the saturation unit is shown in Fig.7.

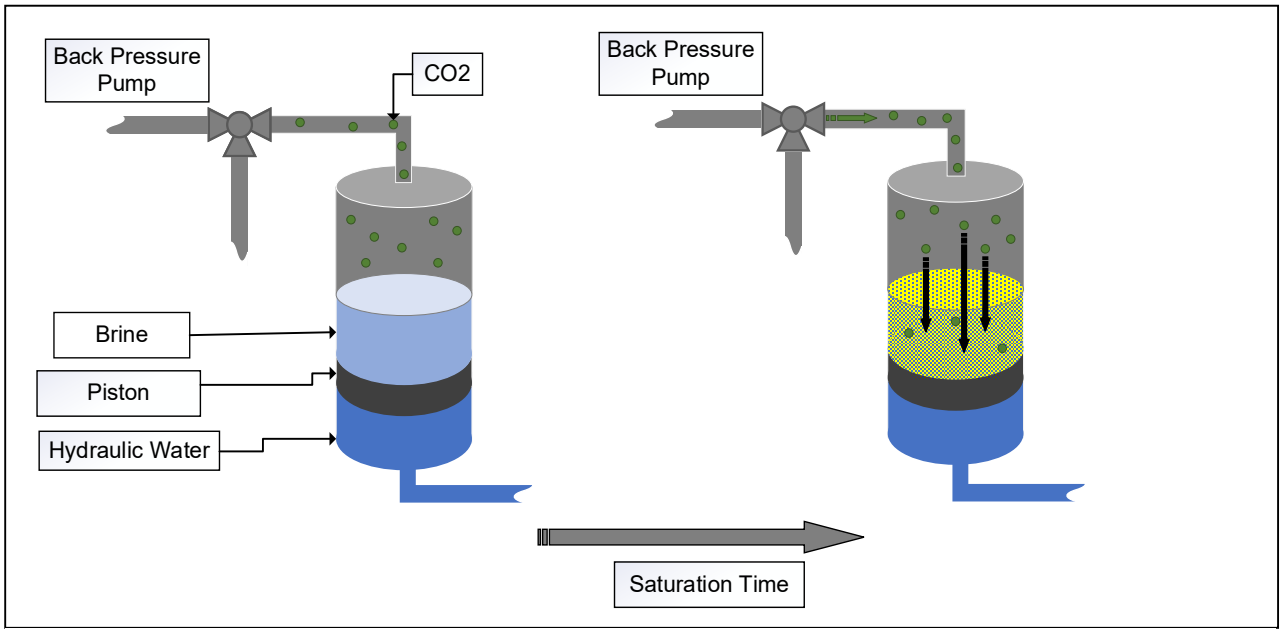

Fig. 7. Design of the integrated saturation unit

3.3.2. Core initialisation process

After the saturation vessel is filled following an overnight saturation period for the fluid sample, the valve linked to the syringe pump is closed. After reaching saturation, the drainage valve on the top shown in Fig. 8 is opened to expel the gas cap prior to the core initialisation. This is done while maintaining the saturation pressure to prevent the dissolved gas from escaping the solution. This pressure is maintained using a syringe pump (back pressure pump) illustrated in Fig.6. Prior to starting the initialisation phase making sure that the saturation vessel only contains the carbonated water, withdrawal of the entire amount of free CO_2 phase from the closed system is important. It is confirmed by having the first liquid droplet appearing at the flush valve shown in Fig.6. After reaching the gas saturated liquid phase, the upper drainage valve is closed.

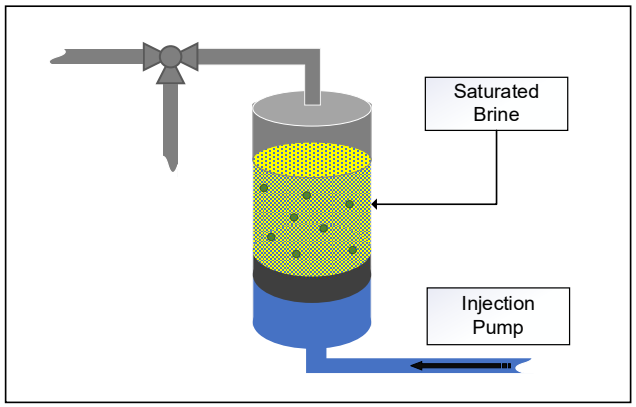

Fig. 8. Fully saturated liquid sample (carbonated water)

Unlike traditional core sample initialisation (100% water saturation) which is done externally in a vacuum chamber, this core initialisation is done inside of a Hassler cell by injecting the carbonated water into the rock directly from the saturation vessel, maintaining the saturation conditions constant. After reaching steady state flow conditions during the initialisation phase, the carbonated water injection stops. After reaching pressure equilibrium along the core, the actual measurement can take place. Moreover, prior to starting the measurement, it is recommended to flush the lines with the displacing fluid (in this case pure CO_2) as they are filled with carbonated water. After eliminating the undesired dead volume of carbonated water from the capillaries, the unsteady state measurement is conducted at saturated and initially undersaturated conditions, with constant injection rate of supercritical CO_2, while recording the differential pressure and cumulative fluid production over time.

4 Results and Discussion

In this section, results for the dynamic viscosity of distilled water and brine samples, both with and without CO_2 are shown first. Then, the USS CO_2 drainage results are presented and discussed.

4.1 Results of viscosity measurements

Fig. 9 shows dynamic viscosity vs. temperature for distilled water and 20% NaCl solution, with and without dissolved CO_2. The impact of dissolved CO_2 on viscosity is more noticeable in distilled water than in the NaCl solution, likely due to reduced CO_2 solubility at higher salinity. Additionally, pressure has an insignificant effect on the viscosity of the 20% NaCl solution, as values at 50 and 80 bar are in a close range.

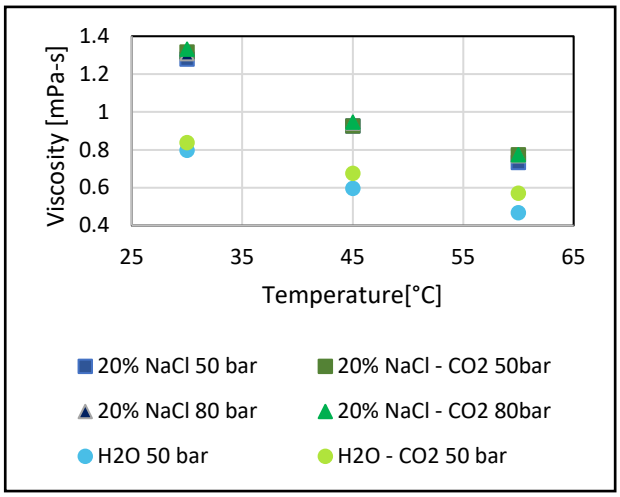

Fig. 9. Brine viscosity; saturated liquid sample (CO_2 saturated)

Since phase mobility depends on relative permeability and viscosity, the impact of dissolved CO_2 on viscosity likely affects relative permeability as well. Higher salinity would also likely diminish the impact of dissolved CO_2 on relative permeability.

4.2 Results of the USS experiments

Preliminary measurements for testing the injectivity and the full functionality of the integrated experimental apparatus have been conducted at ambient and elevated pressure and temperature conditions, with different fluids, namely N_2, H_2, CO_2, distilled water and brine. To validate the functionality of the experimental setup there were two main crucial aspects, the functionality of the fluid saturation cell and the separator for accurate measurement of produced fluid volumes. The main goal is the integration of the liquid saturation unit to maintain the desired conditions for measuring relative permeability of carbonated water and CO_2. The first proof of concept drainage measurement was successfully conducted at 80 bar and 45°C initial conditions where the carbonated water was displaced by supercritical CO_2. The measured irreducible carbonated distilled water saturation was 18%. The saturation was monitored through the produced amount of fluids in the separator and then approximated applying material balance concept, and confirmed by the wet-weight of the core at the end of the flood. Different CO_2 saturation stages and regions during underground CO_2 storage based on solubility values can be identified.

The dissolved amount of CO_2 at different pressure and temperature conditions was approximated from a correlation of solubility of CO_2 with varying reservoir

conditions [25], the data represented was used to determine the different amount of CO_2 dissolved in the water phase. Under laboratory conditions the desired solubility ranges can be reproduced by repeated measurements with varying saturation pressure and temperature conditions. The measurement conditions and results are summarised in Table 3. The CO_2 saturation of the carbonated water is taken from correlation based on the initial pressure and temperature conditions [25].

Table 3. Injection conditions of CO_2 and carbonated water drainage

ID	P	T	CO_2	diss. CO_2	q_{CO2}	S_{wc}
water	bar	°C	kg/ m^3	cc/g	ml/ min	%
saturated	80	45	241	27	1.2	30
under-saturated	80	45	241	20	1.2	40
distilled	80	45	241	0	1.2	40

The drainage measurement with constant total flow rate, in a two-phase system consisting of carbonated distilled water and supercritical CO_2 were successfully conducted at saturated and initially undersaturated conditions, while maintaining the saturation conditions during the initialisation and therefore the fluid properties constant. The measured differential pressures of the saturated and undersaturated CO_2 flood are shown in Fig. 10.

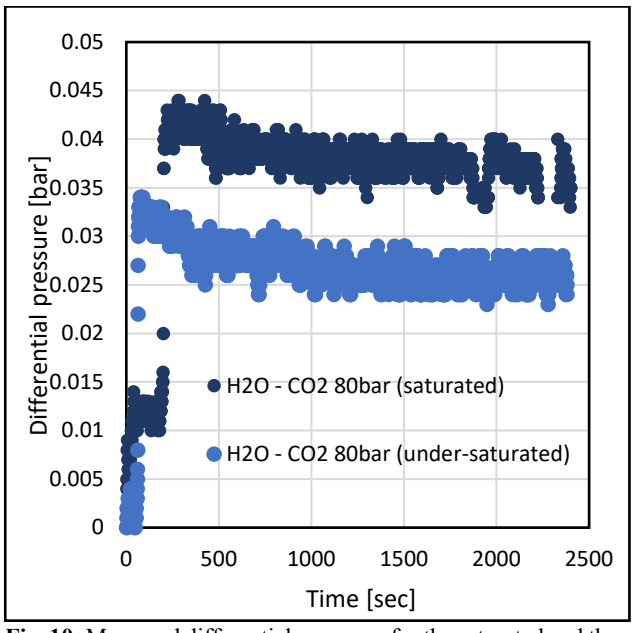

Fig. 10. Measured differential pressures for the saturated and the under-saturated CO_2 flood

Conventional analytical interpretation of laboratory SCAL experiments as performed by many service laboratories may add uncertainty to relative permeability and capillary pressure data and consequently to reservoir simulation. Relative permeability and capillary pressure functions can be obtained more reliably by numerical history matching of displacement experiments. The main limitations of the analytical approach are the crude approximations behind the interpretation models such as the JBN approach, stated in the methodology section. This is the restrictive assumption that neglects action of capillary forces, which is especially a problem close to irreducible saturations. Thus, numerical modelling of SS, USS and centrifuge experiments and more specifically history matching of related production, differential pressure and saturation data are the way to obtain more accurate results because all the physical principles could be considered.

4.3 Numerical interpretation of the USS experiments

The injection schedule and as well as the core sample and fluid properties are listed in Table 4. The history match of the differential pressure and the relative permeability results of both saturated and undersaturated CO_2 flood are shown in Fig.11, 12, 13, 14 respectively. Since there was not enough measured data to match the production very well, Fig. 12 shows the simulated production data.

Table 4. Core sample and fluid properties.

Property	Value
injection rate [ml/min]	1.2
injection time [min]	40
core length [cm]	6
core diameter [cm]	3
core porosity [fraction]	0.25
core permeability [mD]	2000
CO_2 saturated water viscosity @ 50bar; 45°C [cP]	0.6756
CO_2 saturated water viscosity @ 80bar; 45°C [cP]	0.6741
supercritical CO_2 viscosity @ 80bar; 45°C [cP]	0.020771
initial water saturation [fraction]	1

The match was achieved in each case with a combination of manual and assisted history matching by the in-house developed inverse modelling tool based on $DuMu^X$. For the optimisation Powell's [26] method is utilised. It is a direction-set method that performs a series of line searches along various directions, updating directions iteratively. It does not use derivatives and is suitable for optimizing non-smooth and non-convex functions. It builds up a set of directions that span the parameter space, combining information from previous searches [26].
The match at early time is poorer than after breakthrough, which could indicate that the measured pressure difference plot for saturated dataset includes the carbonated water flowing through the inlet dead volume before CO_2 has reach the core. In that case it should be removed from the interpretation. It is included here, since the dead volume was flushed out and the lines were filled with CO_2 in front of the core prior to starting the drainage with CO_2.

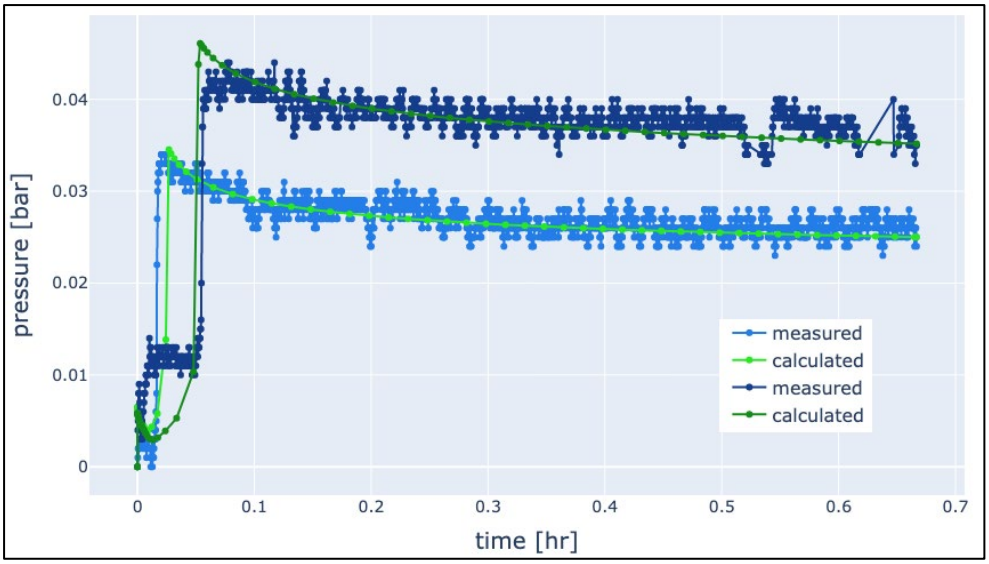

Fig. 11. Measured (blue) and matched (green) differential pressures for the saturated and undersaturated measurements of CO_2 drainage

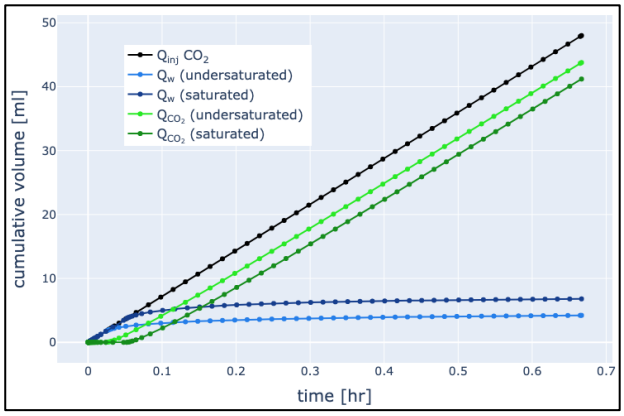

Fig. 12. Cumulative production and injection volumes of the saturated and under-saturated measurements of CO_2 drainage

The relative permeability results are shown in Fig. 13, 14, the brighter shades of green and blue are representing the under-saturated flood and the darker shades correspond to the saturated drainage. The relative permeability results of the saturated CO_2 flood have endpoints of $kr_w^{max} = 0.98$ and $kr_n^{max} = 0.56$, and Corey exponents $c_w = 1.8$ and $c_n = 2.2$ correspondingly, with the remaining water saturation of 30%. The relative permeability results of the undersaturated CO_2 flood have endpoints $kr_w^{max} = 0.88$ and $kr_n^{max} = 0.56$, and Corey exponents $c_w = 3.9$ and $c_n = 2.0$ correspondingly, with the remaining water saturation of 40%. The deviation in the end point saturations from $kr_w^{max} = 1$ is because of the reference absolute permeability. The absolute permeability is set to $k_a = 2000mD$ in the calculation of the relative permeability, because it is a characteristic property of the rock. The lack of in-situ saturation observation through X-ray introduces uncertainty to the measurement and the numerical interpretation method introduces the non-uniqueness of the solution. Therefore, these results should not be viewed isolated as stand-alone values, but analysed with caution and considering the many influencing factors to ensure a comprehensive understanding and accurate conclusions.

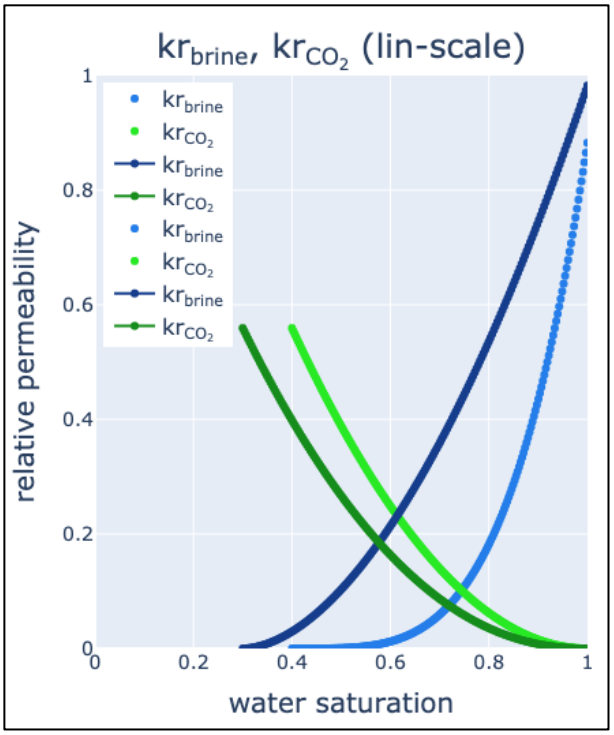

Fig. 13. Comparison between the relative permeability results of saturated and undersaturated CO_2 drainage on linear scale

The comparison between the relative permeability results of saturated and undersaturated CO_2 drainage shows significant difference in the remaining water saturation, and the relative permeability of the water phase. The remaining water saturation is greater when the water is undersaturated in comparison to the case when the water is saturated. It could be because of the mass transfer in the undersaturated core-flood, which could cause the displacement process less efficient. These results indicate that the amount of dissolved CO_2 has an influence on the multiphase flow behaviour. This effect should be verified by running different sets of measurements and benchmarking the results obtained from the measurements to literature data obtained by using

different simulation tools and assisted history matching approaches.

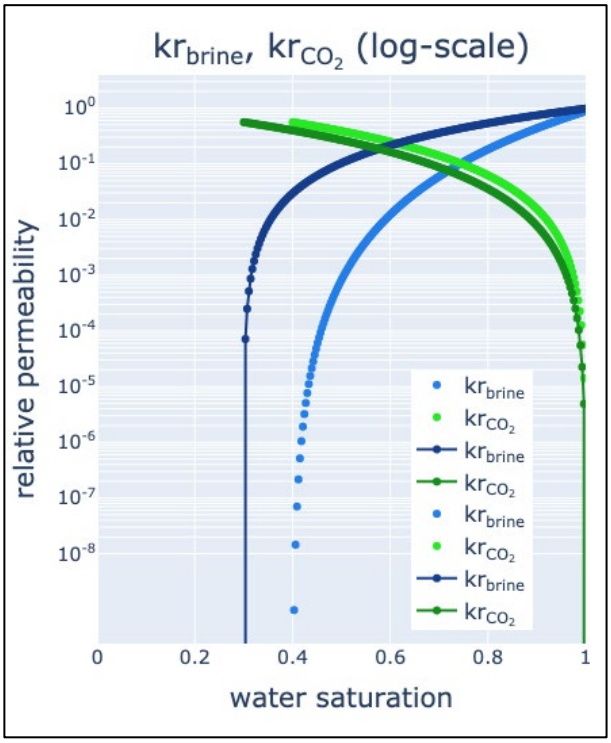

Fig. 14. Comparison between the relative permeability results of saturated and undersaturated CO_2 drainage on logarithmic scale

Further development and extension of the used numerical interpretation tool for estimating relative permeability and capillary pressure curves is crucial. The application of the integrated core-flooding setup and proper data analysis could provide further possibilities to derive mathematical models for the relationship between the multi-phase flow characteristics (saturation functions) and phase behaviour (CO_2 solubility). In order to achieve that and to have a comprehensive set of measurements, the brine saturations are planned to be conducted under pressures of 50bar and 80bar and temperatures of 30°C, 45°C and 60°C systematically with varying salinities up to 200000 ppm. With these chosen conditions a realistic range of dissolved amount of CO_2 in brine can be covered. To reduce the uncertainty of the analysis, experimental determination of relative permeability with the application of microfluidic technology and image analysis is suggested and planned to complement the core-flooding, where a more affordable in-situ saturation monitoring is available via camera, and image analysis [27]. Additionally, in order to reduce the uncertainty and to improve the SCAL interpretation results the following is suggested. Starting point: initial guess from modified analytics - fitting analytics with modified Corey type of curves. Then, separate matching of P_c curve from centrifuge and k_r from SS or USS experiments numerically. As a last resort, the simultaneous matching of several experiments of k_r and P_c numerically. From an optimization point of view, the proposed algorithms by Manasipov (2020) [28] demonstrate the flexibility in terms of representation of relative permeability and capillary pressure curves and it improves the accuracy of interpretation results. Then correlation between the measured properties could be established and generalised with sufficient amount of experiments. It requires using different porous media characteristics such as different pore structures, wettability and various fluid samples based on varying salinity resembling typical prospective reservoirs for geological CO_2 storage. Since, the main goal is to use the measured data in field scale modelling to estimate more reliable CO_2 storage performance. The influence on field scale modelling needs to be addressed and tested simultaneously to the experimental work. As a result, the impact of relative permeability differences in the different saturation zones need to be quantified.

5 Conclusions

Based on the results of this work, two main conclusions can be drawn. The first one is from the experimental point of view and the second one is from the interpretation point of view. The results show the proof of concept that the integrated core-flooding setup including the separator and saturation vessel for two-phase displacement is feasible. The integrated SCAL setup with an extended numerical interpretation tool could be a feasible solution to fill the data gaps or at least to serve as an additional source of information. The recommended future work can be also systematically divided into two main parts accordingly, experimental and computational work. Planned measurement conditions are designed according to the possible dissolved amount of CO_2 in the formation water. To measure the relative permeabilities and capillary pressures of different saturation regions in the flooding zones the solubility values can be mimicked through varying the pressure and temperature conditions. For better accuracy, to improve the interpretation of multiphase flow experiments of supercritical CO_2 drainage, it is planned to extend the applied numerical methods to include mass transfer and compressibility.

Acknowledgements

The authors would like to express their gratitude to Manfred Stövesand for his constant support.

References

1. UNFCCC, Https://Unfccc.Int/Files/Essential_background/Convention/Application/Pdf/English_paris_agreement.Pdf. [Accessed: 24-Jun-2024]. 3 (2015).
2. J. Moore, P. Holcomb, D. Crandall, S. King, J. H. Choi, S. Brown, and S. Workman, Adv Water Resour **153**, 103953 (2021).
3. S. Berg, S. Oedai, and H. Ott, International Journal of Greenhouse Gas Control **12**, 478 (2013).

4. S. Berg, H. Dijk, E. Unsal, R. Hofmann, B. Zhao, and V. Raju Ahuja, Comput Geotech **168**, 106091 (2024).
5. S. Benson, R. Pini, C. Reynolds, and S. Krevor, 51 (2013).
6. S. M. Benson, F. Hingerl, L. Zuo, R. Pini, K. S. C. Reynolds, B. Niu, R. Calvo, and A. Niemi, Global CCS Institute 1 (2015).
7. N. Müller, Transp Porous Media **87**, 367 (2011).
8. S. C. M. Krevor, R. Pini, L. Zuo, and S. M. Benson, Water Resour Res **48**, 1 (2012).
9. X. Chen, A. Kianinejad, and D. A. DiCarlo, Proceedings - SPE Symposium on Improved Oil Recovery **3**, 1504 (2014).
10. G. S. Jeong, S. Ki, D. S. Lee, and I. Jang, Sustainability (Switzerland) **13**, 1 (2021).
11. J. Ge, X. Zhang, J. Liu, A. Almutairi, and F. Le-Hussain, Fuel **321**, 124132 (2022).
12. S. Pesch, S. Schulz, N. Aboud, and M. Schlüter, J Chem Eng Data **66**, 2355 (2021).
13. C. McPhee, J. Reed, and I. Zubizarreta, Developments in Petroleum Science **64**, 1 (2015).
14. B. S. E Buckley, M. C. Leverett, and M. Aime, Transactions of the AIME **146**, 107 (1942).
15. E. F. Johnson, D. P. Bossler, and V. O. N. Bossler, Transactions of the AIME **216**, 370 (1959).
16. R. Manasipov and B. Jenei, Https://Github.Com/Coreflowlab/Tutorials (2024).
17. R. Helmig, Multiphase Flow and Transport Processes in the Subsurface (1997).
18. J. G. Maas, SCA2011-08 (2011).
19. T. Koch, D. Gläser, K. Weishaupt, S. Ackermann, M. Beck, B. Becker, S. Burbulla, H. Class, E. Coltman, S. Emmert, T. Fetzer, C. Grüninger, K. Heck, J. Hommel, T. Kurz, M. Lipp, F. Mohammadi, S. Scherrer, M. Schneider, G. Seitz, L. Stadler, M. Utz, F. Weinhardt, and B. Flemisch, Computers & Mathematics with Applications **81**, 423 (2021).
20. B. Flemisch, M. Darcis, K. Erbertseder, B. Faigle, A. Lauser, K. Mosthaf, S. Müthing, P. Nuske, A. Tatomir, M. Wolff, and R. Helmig, Adv Water Resour **34**, 1102 (2011).
21. R. Manasipov, Https://Pypi.Org/Project/Coreflow/ (2024).
22. S. Berg, H. Dijk, E. Unsal, R. Hofmann, B. Zhao, and V. Raju Ahuja, Comput Geotech **168**, 106091 (2024).
23. R. Lenormand, K. Lorentzen, J. G. Maas, and D. Ruth, SCA2016-006 (2016).
24. R. Lenormand, K. Lorentzen, J. G. Maas, and D. Ruth, Petrophysics **58**, 48 (2017).
25. R. Wiebe and V. L. Gaddy, J Am Chem Soc **62**, 815 (1940).
26. M. J. D. Powell, Comput J **7**, 155 (1964).
27. B. Jenei, R. Manasipov, N. Langanke, and H. Samara, Society of Petroleum Engineers - SPE Reservoir Characterisation and Simulation Conference and Exhibition 2023, RCSC 2023 (2023).
28. R. Manasipov and B. Jenei, Society of Petroleum Engineers - SPE Europec Featured at 82nd EAGE Conference and Exhibition (2020).